



# Anemarsaponin B mitigates acute pancreatitis damage in mice through apoptosis reduction and MAPK pathway modulation

YI HU<sup>1,#</sup>; ZHONGYANG REN<sup>2,#</sup>; ZHENGZHONG ZHAO<sup>1</sup>; YONGJIA HUANG<sup>3</sup>; WANTING HUANG<sup>3</sup>; JIE LIU<sup>3,\*</sup>; LING DING<sup>3,\*</sup>

<sup>1</sup> Gastroenterology Department, Chongqing University Jiangjin Hospital, Jiangjin Central Hospital of Chongqing, Chongqing, China

<sup>2</sup> Surgical Department, Chongqing Jiangjin District Hospital of Chinese Medicine, Chongqing, China

<sup>3</sup> Pharmacy Department, Chongqing University Jiangjin Hospital, Jiangjin Central Hospital of Chongqing, Chongqing, China

**Key words:** Anemarsaponin B, Acute pancreatitis, Cytokines, MAPK, TRAF6, Gut flora

**Abstract: Background:** Acute pancreatitis (AP), known for its rapid onset and significant incidence and mortality rates, presents a clinical challenge due to the limited availability of effective treatments and preventive measures. Anemarsaponin B (ASB) has emerged as a potential therapeutic agent, demonstrating capabilities in reducing immune inflammation, positioning it as a promising candidate for AP treatment. **Methods:** We investigated the effects of ASB on AP in mice, induced by caerulein and lipopolysaccharide (LPS). Peripheral blood samples were collected 24 h post-induction with caerulein to assess of key biomarkers including lipase, amylase, TNF- $\alpha$ , IL-1 $\beta$ , IL-6, SOD, and GSH-Px. A range of techniques such as immunohistochemistry staining, immunofluorescence staining, Western blotting, and quantitative Polymerase Chain Reaction (q-PCR), were employed to measure the expression of critical genes. Additionally, pancreas samples from the mice were harvested for microbiome and metabolome sequencing, with the data analyzed to understand the impact of ASB on AP. **Results:** Our study revealed that, compared to the sham group, the AP group exhibited significantly higher serum levels of lipase, amylase, and cytokines, while levels of SOD and GSH Px were notably lower. Treatment with ASB led to a substantial decrease in the levels of lipase, amylase, and cytokines, and an increase in SOD and GSH-Px levels. q-PCR analysis of pancreatic histiocytes corroborated these serum findings. Hematoxylin and Eosin (H&E) staining indicated significant alterations in the pathological changes in the pancreas, lungs, and small intestine of the AP model due to ASB. Immunofluorescence assays demonstrated that ASB alleviated the apoptosis of pancreatic histiocytes in the AP model. Western Blot and histological analyses showed that ASB reduced the phosphorylation of TAK, p38, JNK, and ERK proteins, as well as the levels of TRAF6 protein in the AP model. Furthermore, metabolomic and gut microbiota analysis identified 27 differential metabolites and 34 differential species. The combined metabolome and microbiome analysis suggested an association between certain microbes (e.g., unclassified-Saprospiraceae and unclassified-Micavibrionales) and metabolites (e.g., LysoPE (0:0/20:0), PC (DiMe(13,5)/PGJ2)), and Heptanoic acid, indicating potential pathways through which ASB may exert its therapeutic effects in AP. **Conclusions:** ASB exhibits therapeutic efficacy in treating AP induced by caerulein combined with lipopolysaccharide (LPS), primarily through modulating the mitogen-activated protein kinase (MAPK) signaling pathway. This discovery offers fresh perspectives for AP drug development, underscoring the potential of targeting specific cellular pathways. Additionally, the intricate interplay observed between the gut microbiota and metabolites following ASB treatment highlights novel therapeutic targets, suggesting that manipulating the gut microbiome and metabolome could be a viable strategy in AP management. These findings pave the way for further research into comprehensive treatment approaches that incorporate both pharmacological intervention and microbiota modulation.

\*Address correspondence to: Jie Liu, renxiaoen@cqu.edu.cn;  
Ling Ding, dling2022@126.com

#These authors Yi Hu and Zhongyang Ren contributed equally to this work

Received: 28 December 2023; Accepted: 11 March 2024;

Published: 06 May 2024

## Abbreviations

AP	Acute pancreatitis
ASB	Anemarsaponin B
TB-II	Timosaponin B-II
LPS	Lipopolysaccharide
TNF- $\alpha$	Tumor necrosis factor alpha



IL-1 $\beta$	Interleukin 1 beta
IL-6	Interleukin 6
IL-1-R	Interleukin 1 receptor
SOD	Superoxide dismutase
GSH-Px	Glutathione peroxidase
H&E	Hematoxylin-eosin staining
TAK	TGF-beta activated kinase
p38	Mitogen-activated protein kinase 14 or p38 kinase
JNK	Mitogen-activated protein kinase 8 or c-Jun N-terminal kinase
ERK	Mitogen-activated protein kinase 1 or extracellular regulated MAP kinase
TRAF6	TNF receptor associated factor 6
MAPK	Mitogen-activated protein kinase
SBA	Secondary bile acid
RTK	Receptor Tyrosine Kinase

## Introduction

Acute pancreatitis (AP) is a prevalent acute abdominal condition in clinical settings and is a leading cause of hospital admissions related to gastrointestinal disorders [1]. The high incidence and mortality rates of AP, including its acute phase and complications, necessitate prompt diagnosis and treatment, highlighting its critical importance for human health [2]. Research has identified various causes of AP, such as pancreatic duct obstruction from gallstones, alcohol consumption, endoscopic retrograde cholangiopancreatography, and drug-induced cellular and organelle dysfunction [3]. Over the last decade, factors such as aberrant calcium signaling [4,5], mitochondrial dysfunction, premature activation of trypsinogen [6,7], and endoplasmic reticulum stress [8] have been recognized as key contributors to acinar cell necrosis. This cellular damage leads to the release of chemokines, cytokines, and adhesion molecules, which recruit immune cells to the site of injury, triggering a systemic inflammatory response that exacerbates pancreatic and distal organ damage, culminating in AP [9,10].

Recent studies suggest a possible link between the global obesity epidemic and the rising incidence and mortality of AP worldwide [11], underscoring the urgent need to develop effective therapeutic interventions for treating or preventing AP. In the later stages of AP, complications such as intestinal dysfunction and pancreatic necrosis often occur. Notably, the bacteria responsible for infections in pancreatic necrosis primarily originate from the intestinal flora, including species like *Escherichia coli* and *Enterococcus*. This points to the significant role of the intestinal microbiota in the onset and progression of AP, emphasizing the need for a deeper understanding of this interaction [12].

Exploring Traditional Chinese Medicine (TCM) offers a promising avenue for the development of treatments for AP, particularly given the current scarcity of effective drugs and TCM's renowned anti-inflammatory properties. *Anemarrhena asphodeloides* Bge, a traditional Chinese herb derived from the dried rhizome of the same plant, is known

for its properties of clearing heat, purging fire, nourishing yin, and moistening dryness. This herb is extensively used in traditional Chinese medicine in China and Southeast Asian countries. Anemarsaponin B (ASB), an active compound extracted from the dried rhizomes of *Anemarrhena asphodeloides* [13], has shown potential in osteoporosis prevention [14], anti-inflammatory effects [15], and anti-thrombotic properties [16]. Kim et al. reported that ASB effectively reduces the secretion of inflammatory factors TNF- $\alpha$  and IL-6 by macrophages and inhibits the activation of the p38 MAPK signaling pathway [15]. Currently, research on ASB is limited to the aforementioned reports. However, there is abundant research on Timosaponin B-II (TB-II), a chemically related saponin extract from *Anemarrhena asphodeloides*. TB-II [15] undergoes a dehydration reaction on a specific pentacyclic ring, where one hydroxyl group (-OH) and an adjacent hydrogen atom are removed, forming a carbon-carbon double bond, resulting in the chemical structure of ASB [13]. Current research highlights TB-II's antioxidant [17,18], anti-inflammatory [19], anti-dementia, and cardioprotective properties [20].

Based on the above, ASB demonstrates significant anti-inflammatory potential; however, there are currently no reported studies conducted in animal models or more complex systems. Simultaneously, the effects of ASB on the microbial flora during AP remain unexplored. Given this gap in knowledge, our study aims to investigate the therapeutic potential of ASB in AP, utilizing a model induced by caerulein and LPS. This research could provide crucial insights into the role of ASB in modulating gut microbiota and its overall impact on the treatment of AP.

## Materials and Methods

### Materials

**Animals:** Thirty specific pathogen-free (SPF) C57BL/6J mice (Si Pei Fu Biotechnology Co., Ltd., Quanzhou, Fujian, China), aged between 6–8 weeks. The animal experimentation was conducted under the license number SCXK (Beijing, China) 2019–2010. Prior to the commencement of experiments, all mice were allowed a 7-day acclimatization period in an environment maintained at a temperature of 22°C–24°C and subjected to a 12-h light/dark cycle. During the entire duration of the experiment, the mice were provided with standard laboratory feed and had access to drinking water *ad libitum*. All experimental animals in this project must comply with Chongqing Liangjiang New District's ethical standards, authorized by approval number IV/S-SYDW-045, ensuring their welfare and ethical treatment.

**Reagents:** Anemarsaponin B (ASB) (139051-27-7, Weikeyi, Chengdu, Sichuan, China) was acquired from Sichuan Weikeyi Biological Technology Co., Ltd. The antibodies for TRAF6 (AF5376), TAK1 (AF6019), p-TAK1 (AF3019), p-P38 (AF4001), JNK 1/2/3 (AF6319), p-JNK 1/2/3 (AF3318), ERK1/2 (AF0155), p-ERK1/2 (BF8004), IL-1 $\beta$  (AF5103), TNF- $\alpha$  (AF7014), IL-6 (DF6087), Cleaved Caspase 3 (AF7022) and  $\beta$ -actin (AF7018) were sourced from Affinity Biosciences Co., Ltd., Wuhan, Hubei, China.

Additionally, the antibody against P38 was acquired from ZENBIO (R25239) in China. Furthermore, ELISA kits for measuring IL-6 (SYP-M0031), TNF- $\alpha$  (SYP-M0036), IL-1 $\beta$  (RX203063M), Lipase (RX200206M) and  $\alpha$ -amylase (RX200929M) were procured from Ruixin Biological Technology Co., Ltd., Quanzhou, Fujian, China.

#### *Model of acute pancreatitis (AP) and drug treatment*

The mice were randomly allocated into five groups. These included a control group, a model group, and three treatment groups receiving low (20 mg/kg), medium (40 mg/kg), and high (80 mg/kg) doses of ASB. The AP modeling method is as reported before [21,22]. The mice were fasted but had free access to water for 12 h prior to the induction of the AP model. The model was established by administering injections of Caerulein (C860403, Macklin, Shanghai, China) at a dosage of 100  $\mu$ g/kg, given hourly for a total of six consecutive injections. Subsequently, an injection of Lipopolysaccharide (LPS) (CL6891, Coolaber, Beijing, China) at a dose of 20 mg/kg was administered following the final Caerulein injection. The control group received injections of an equal volume of normal saline at the same time intervals. One hour and nine hours after the model induction, the treatment groups received ASB at their respective dosages, while the control and model groups were administered an equivalent volume of normal saline.

#### *Sample collection*

24 h after inducing AP, the mice were anesthetized, and blood samples were collected using the eyeball enucleation method. Subsequently, the mice were euthanized via cervical dislocation, and their pancreas tissues were extracted through an abdominal incision. The harvested tissues were first rinsed with normal saline and then divided into four equal parts. One part was fixed in 4% paraformaldehyde (BL538A, Biosharp, Guangzhou, Guangdong, China) for 24 h, followed by triple rinsing in normal saline. This sample was then dehydrated, treated for transparency, and embedded in paraffin (39601006, Leica, Wetzlar, Hessen, Germany). Two of the tissue samples were placed in 2 mL cryotubes, immediately frozen in liquid nitrogen, and stored at  $-80^{\circ}\text{C}$  for further analysis. The remaining tissue sample was utilized for wet and dry weight measurements to assess tissue edema.

#### *ELISA*

The blood serum was separated from the collected blood samples of all mice by centrifugation at 5000 g for 10 min. Following the manufacturer's protocols, the concentrations of  $\alpha$ -amylase, lipase, IL-1 $\beta$ , IL-6, and TNF- $\alpha$  in the mouse serum were determined. These measurements were conducted using a spectrophotometer (BioTek, SYNERGY/H1, Winooski, Vermont, USA). This process enabled the quantification of these biomarkers, which are crucial for assessing the severity and inflammatory status of AP in the mice.

#### *The wet weight to dry weight (W/D) ratio of pancreas*

The harvested pancreas tissue was initially rinsed with normal saline and then gently blotted with filter paper to remove any

surface moisture. The wet weight of the tissue was accurately measured using an electronic analytical balance (ME303T, METTLER TOLEDO, Greifensee, Zurich Canton, Switzerland). After weighing, the tissue was placed in a constant temperature drying oven (OGS60, Thermo Scientific, Waltham, Massachusetts, USA) and maintained at  $80^{\circ}\text{C}$  for 48 h to ensure thorough drying. Following this drying period, the dry weight of the tissue was again measured using the electronic analytical balance. To assess tissue edema, the wet-to-dry weight ratio of the pancreas tissue was calculated by dividing the wet weight by the dry weight. This ratio provides an important quantitative indicator of the degree of inflammation and edema in the pancreas tissue, which are key parameters in evaluating the severity of AP.

#### *H&E staining*

The mouse pancreas tissue slices were subjected to Hematoxylin and Eosin (H&E) staining using an H&E staining kit (G1120, Solarbio, Beijing, China). The staining process began with incubating the tissue slices in hematoxylin solution for 3 min at room temperature. Subsequently, the slices were rinsed with running water before being briefly immersed in 1% hydrochloric acid ethanol for 5 s. After another rinse with running water, the slices were stained with eosin solution for 3 min at room temperature. Following the staining process, the tissue slices underwent dehydration and were made transparent using a specific solution (G8590, Solarbio, Beijing, China). The slides were then sealed with neutral gum to preserve the stained tissue. The staining results, revealing the microscopic architecture and any pathological changes within the pancreas tissue, were captured and examined using a microscope (Leica, DMi8, Wetzlar, Hessen, Germany). This histological examination is crucial for assessing the extent of inflammation and tissue damage in the context of AP.

#### *Immunohistochemistry*

The pancreas tissue slices from the mice were prepared for immunohistochemistry as follows: Initially, the tissue slices were treated with 0.1% Triton X-100 (ST795, Beyotime, Shanghai, China) at room temperature for 15 min to permeabilize the cell membranes. Subsequently, they were immersed in a solution containing 3% hydrogen peroxide for 5 min to quench endogenous peroxidase activity, followed by thorough washing with phosphate-buffered saline (PBS) to remove any residual reagents. The slices were then subjected to antigen retrieval by boiling in sodium citrate antigen repair solution (D0081, Beyotime, Shanghai, China). After this step, the slices were incubated in goat serum (C-0005, Bioss, Woburn, Massachusetts, USA) at room temperature for 1 h to block non-specific binding. This was followed by the addition of the primary antibody, applied dropwise according to the specific instructions provided for each antibody. The tissue slices were then incubated overnight at  $4^{\circ}\text{C}$  with the primary antibody. The following day, the tissue slices were washed with PBS and incubated with a secondary antibody (PV9001, ZSGB-BIO, Beijing, China) for 30 min at  $37^{\circ}\text{C}$  in

a dark environment. Subsequently, color development was achieved using a DAB staining kit (ZLI-9018, ZSGB-BIO, Beijing, China). After rinsing with water, the nuclei were counterstained with 0.1% nuclear fast red solution (G1320, Solarbio, Beijing, China) for enhanced contrast. Finally, the tissue slices were dehydrated, cleared, and sealed for preservation. The results of the immunohistochemical staining were captured and analyzed using a microscope (DMi8, Leica, Wetzlar, Hessen, Germany). This process is essential for visualizing specific antigen-antibody interactions within the tissue, thereby providing valuable insights into the molecular and cellular changes occurring in the pancreas during AP.

#### Western blot

The pancreatic tissue samples from the mice were processed for Western blot analysis as follows: First, the tissue was thoroughly ground and homogenized, followed by lysis using Western and IP lysis buffer (P0013, Beyotime, Shanghai, China). Proteins were then denatured by boiling them in 5x SDS-PAGE loading buffer (P0015L, Beyotime, Shanghai, China) at 100°C for 10 min. After denaturation, the proteins were separated using 10% SDS-PAGE at a constant voltage of 100 V. The separated proteins were then transferred onto a polyvinylidene fluoride membrane using a constant current of 200 mA. To prevent non-specific binding, the membrane was blocked with 5% bovine serum albumin for 1 h at room temperature. After blocking, the membrane was incubated overnight at 4°C with the primary antibodies, which were diluted according to the manufacturer's instructions. Following the primary antibody incubation, the membrane was incubated with a goat anti-rabbit IgG (H + L) HRP-linked secondary antibody (S0001, Affinity, Wuhan, Hubei, China) for 2 h at room temperature. The protein bands were then visualized using a highly sensitive Chemiluminescent Substrate Kit (PA134-01, Biomed, Shanghai, China). The chemiluminescent signals were captured and imaged using a high-sensitivity multifunctional imager (Amersham ImageQuant 800, Cytiva, Marlborough, Massachusetts, USA). This Western blot analysis is crucial for detecting specific proteins and post-translational modifications, providing insights into the molecular pathways involved in the mouse model of AP.

TABLE 1

The primer sequences of cytokine genes for quantitative real-time PCR detection

Primer ( <i>Homo sapiens</i> )	Sequence from 5' to 3'
IL1 $\beta$ -F	GAAATGCCACCTTTTGACAGTG
IL1 $\beta$ -R	TGGATGCTCTCATCAGGACAG
IL6-F	CTGCAAGAGACTTCCATCCAG
IL6-R	AGTGGTATAGACAGGCTGTGG
TNF $\alpha$ -F	CTGAACTTCGGGGTGATCGG
TNF $\alpha$ -R	GGCTTGCTCACTCGAATTTTGAGA

#### Quantitative real-time PCR

The pancreas tissue from the mouse was ground into a fine homogenate, and total RNA was extracted from the homogenized pancreas tissue using the TRNzol Universal Reagent (DP424, Tiangen, Beijing, China). The extracted RNA was then converted into complementary DNA (cDNA) using the reverse transcription kit (RR047A, Takara, Kusatsu, Higa Prefecture, Japan). The reverse transcription was performed strictly following the manufacturer's protocol. Real-time fluorescence quantitative PCR was conducted using the SYBR Green Realtime PCR Master Mix Kit (QPK-212, TOYOBO, Osaka, Japan). The Touch Real-Time PCR Detection System (CFX96, Bio-Rad, Hercules, California, USA) was utilized to detect and analyze the PCR results. In this analysis,  $\beta$ -actin was used as an internal reference gene to normalize the expression data. The sequence of primers is as follows (Table 1).

#### Immunofluorescence technique

The mouse pancreatic tissue samples were fixed in paraformaldehyde (BL539A, Biosharp, Guangzhou, Guangdong, China) to preserve cellular structure and integrity. This was followed by dehydration using Sucrose (G66841B, Greagent, Shanghai, China), thin tissue sections were then obtained using a frozen microtome. For immunostaining, these sections were incubated with a primary antibody against Cleaved Caspase-3 (AF7022, Affinity, Wuhan, Hubei, China) for 24 h. After primary antibody incubation, Alexa Fluor 555/488 labeled rabbit secondary antibody (bs-0312R-AF555, Bioss, Woburn, Massachusetts, USA) was applied to bind to the primary antibody. Additionally, DAPI (C1006, Beyotime, Shanghai, China) was used for nuclear staining. The stained sections were then sealed with an anti-fluorescence quenching solution (P0126, Beyotime, Shanghai, China) to preserve the fluorescence signal. The final observation and analysis of the stained tissue sections were conducted using a fluorescence microscope (Leica, DMi8, Wetzlar, Hessen, Germany).

#### Microbiomics and untargeted metabolomics sequencing

Pancreatic tissue samples were meticulously collected from three groups of mice: the sham group, the AP group, and the group treated with ASB at a dosage of 40 mg/kg. These samples were immediately frozen to preserve their biochemical integrity and stored at -80°C to ensure optimal conditions for later analysis. For comprehensive microbiomic and metabolomic profiling, the samples were sent to Biomarker Technologies Company in Beijing, China. Upon receiving the data, it underwent thorough omics analyses, both separately and in an integrated manner. This approach allowed for a detailed examination of the microbiome and metabolome changes in the pancreatic tissue, offering valuable insights into the biological impact of ASB on AP and the potential interplay between microbiomic and metabolomic alterations.

#### Statistical analysis

Statistical analysis was conducted by quantifying the images with ImageJ Pro Plus and performing comparisons using Prism (Graphpad Software Inc, GraphPad 8.0.1, San Diego,

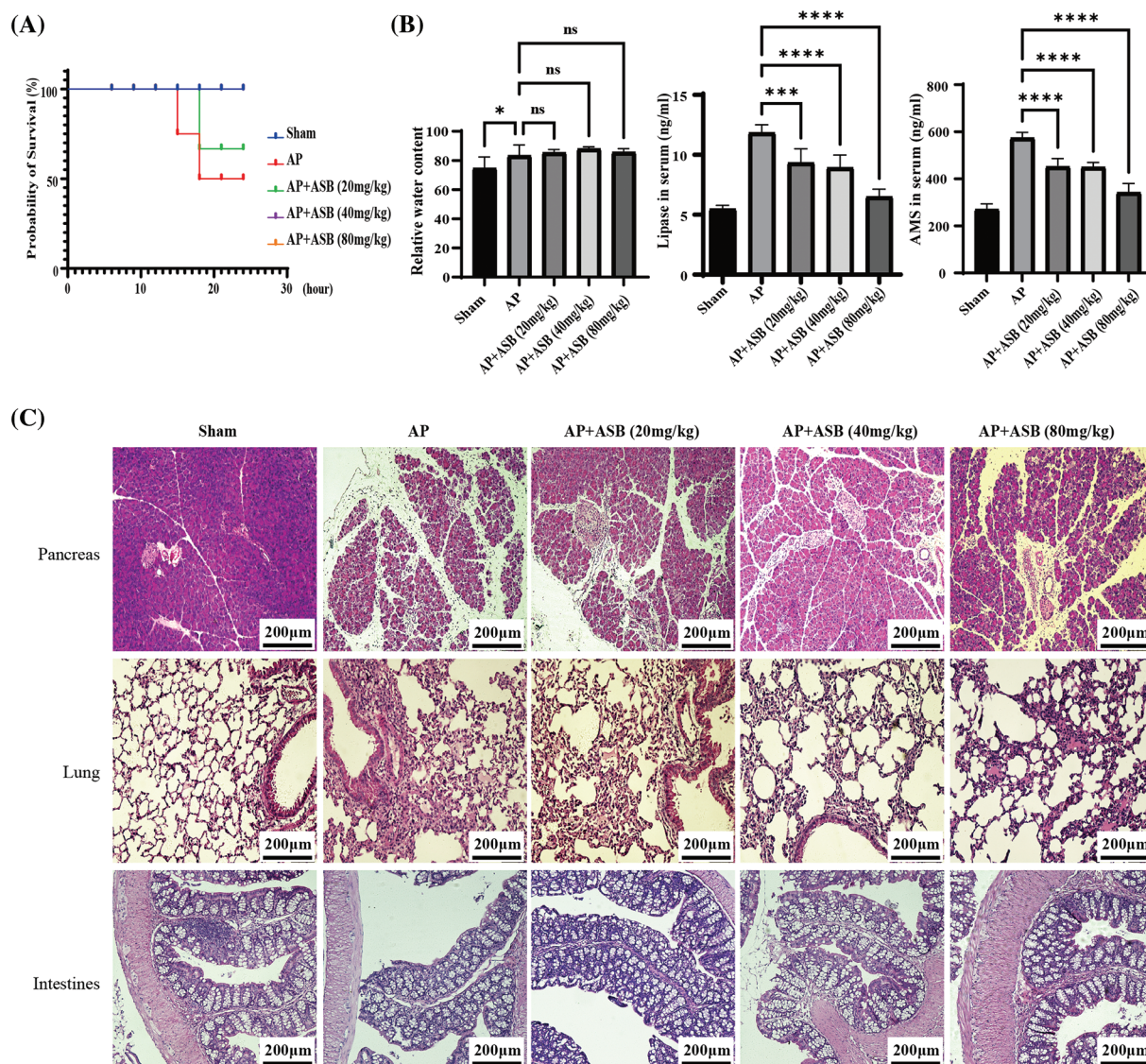


**FIGURE 1.** ASB alleviates caerulein and LPS-induced pancreatitis in mice. (A) Survival curve 24 h post-model establishment. No fatalities were observed in the (40) and (80 mg/kg) dose groups, resulting in their curves overlapping with the Sham group. (B) Pancreatic water content, serum lipase, and amylase levels. (C) HE staining of pancreas, lungs, and intestines before and after ASB treatment. “ns” denotes no significant difference,  $*p < 0.05$ ,  $***p < 0.001$ ,  $****p < 0.0001$ . AP, acute pancreatitis model. Scale bar = 200  $\mu\text{m}$  ( $n = 6$  mice per group).

California, USA). The data was presented as mean  $\pm$  SD, and one-way ANOVA with Dunnett’s multiple comparison test was applied to assess the statistical significance of group differences.  $*p < 0.05$  was considered to indicate a statistically significant difference.

## Results

### *Anemarsaponin B (ASB) alleviates pancreatitis induced by caerulein and LPS in a mouse model*

In our study, the acute pancreatitis (AP) mouse model was successfully induced using a combination of caerulein and lipopolysaccharide (LPS), validated by observations of the 24-h survival rate and pancreatic water content. The AP model exhibited a mortality rate of 50% (12 out of 24 mice) within the first 24 h. Interestingly, the group treated with 20 mg/kg ASB exhibited a mortality rate of 36%, while no mortality was observed in the groups receiving higher dosages of ASB (Fig. 1A). This indicates a significant

protective effect of ASB against early mortality in AP. Regarding pancreatic water content, the ASB treatment groups showed no statistically significant difference compared to the AP group ( $p > 0.05$ ), suggesting that ASB does not markedly affect edema in this model (Fig. 1A). However, serum analysis revealed a notable reduction in esterase and amylase levels across all ASB-treated groups compared to the AP group ( $p < 0.01$ ) (Fig. 1B), indicating a potential therapeutic effect of ASB on pancreatic enzyme levels. Histological examination of the pancreatic tissues using Hematoxylin and Eosin (H&E) staining revealed stark differences. The sham group displayed normal pancreatic morphology with intact lobules and no inflammation. In contrast, the AP group showed disrupted pancreatic architecture, including widened interlobular spaces, disorganization, and significant inflammatory infiltration (Fig. 1C). Interestingly, ASB treatment, particularly at 40 and 80 mg doses, showed noticeable improvements in pancreatic tissue structure. In the lung

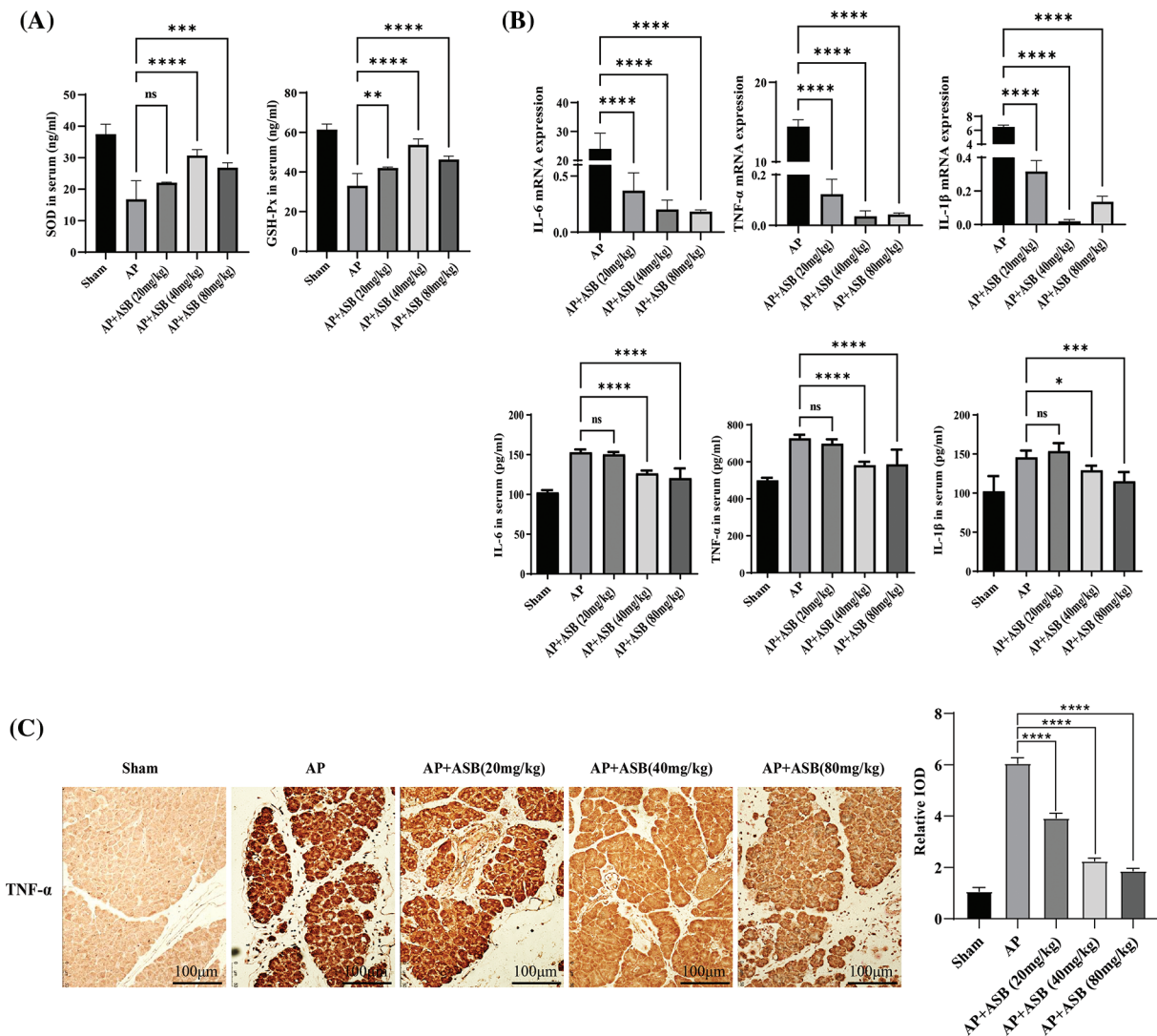


**FIGURE 2.** ASB modulates inflammatory and redox factors in mouse acute pancreatitis. (A) Serum levels of SOD and GSH redox factors assessed by ELISA. (B) Quantitative analysis of serum IL-1 $\beta$ , IL-6, and TNF- $\alpha$  levels using ELISA, alongside qPCR results for gene expression in pancreatic tissues. In qPCR results, the Sham group, serving as the reference point (normalized to 1), does not have a corresponding bar graph. (C) Immunohistochemical staining of TNF- $\alpha$  in pancreatic tissue. “ns” denotes no significant difference, \* $p$  < 0.05, \*\* $p$  < 0.01, \*\*\* $p$  < 0.001, \*\*\*\* $p$  < 0.0001. Scale bar = 100  $\mu$ m (n = 6 mice per group).

tissues, the sham group exhibited normal alveolar architecture, while the AP group exhibited thickened alveolar walls, congestion, and inflammatory infiltration, indicative of secondary lung damage. The ASB-treated groups, especially at higher doses, showed marked improvement in lung tissue structure compared to the AP group. Furthermore, the AP model impacted the villi in the small intestine (jejunum-ileum segment), with ASB treatment demonstrating protective effects. However, the impact on the large intestine villi was less pronounced (Fig. 1C). These findings highlight the potential of ASB in mitigating the systemic effects of AP.

#### ASB modulates inflammatory and redox factors in a mouse model of AP

This study utilized quantitative PCR (qPCR) to evaluate the impact of ASB on inflammatory markers, specifically IL-1 $\beta$ , IL-6, and TNF- $\alpha$ , in the pancreas of mice with experimentally induced AP. In parallel, ELISA tests were

conducted to measure the levels of these inflammatory factors as well as redox factors (SOD and GSH-Px) in the serum. As shown in Figs. 2A and 2B, the induction of AP using caerulein and LPS significantly decreased the levels of SOD and GSH-Px ( $p$  < 0.01), while markedly increasing serum concentrations of IL-1 $\beta$ , IL-6, and TNF- $\alpha$  ( $p$  < 0.01). Notably, treatment with ASB, particularly at doses of 40 mg or higher, led to a significant decrease in the expression of these inflammatory cytokines and an increase in SOD and levels in the serum ( $p$  < 0.01). These alterations in serum cytokine levels were in agreement with the qPCR results from pancreatic tissues. Additionally, immunohistochemistry (IHC) analysis of pancreatic TNF- $\alpha$  supported these findings, showing increased expression in the AP model group and a notable reduction in the ASB-treated groups, thus corroborating the serum test results (Fig. 2C). This consistency across various testing methods underscores the potential anti-inflammatory and antioxidative effects of ASB in the context of AP.

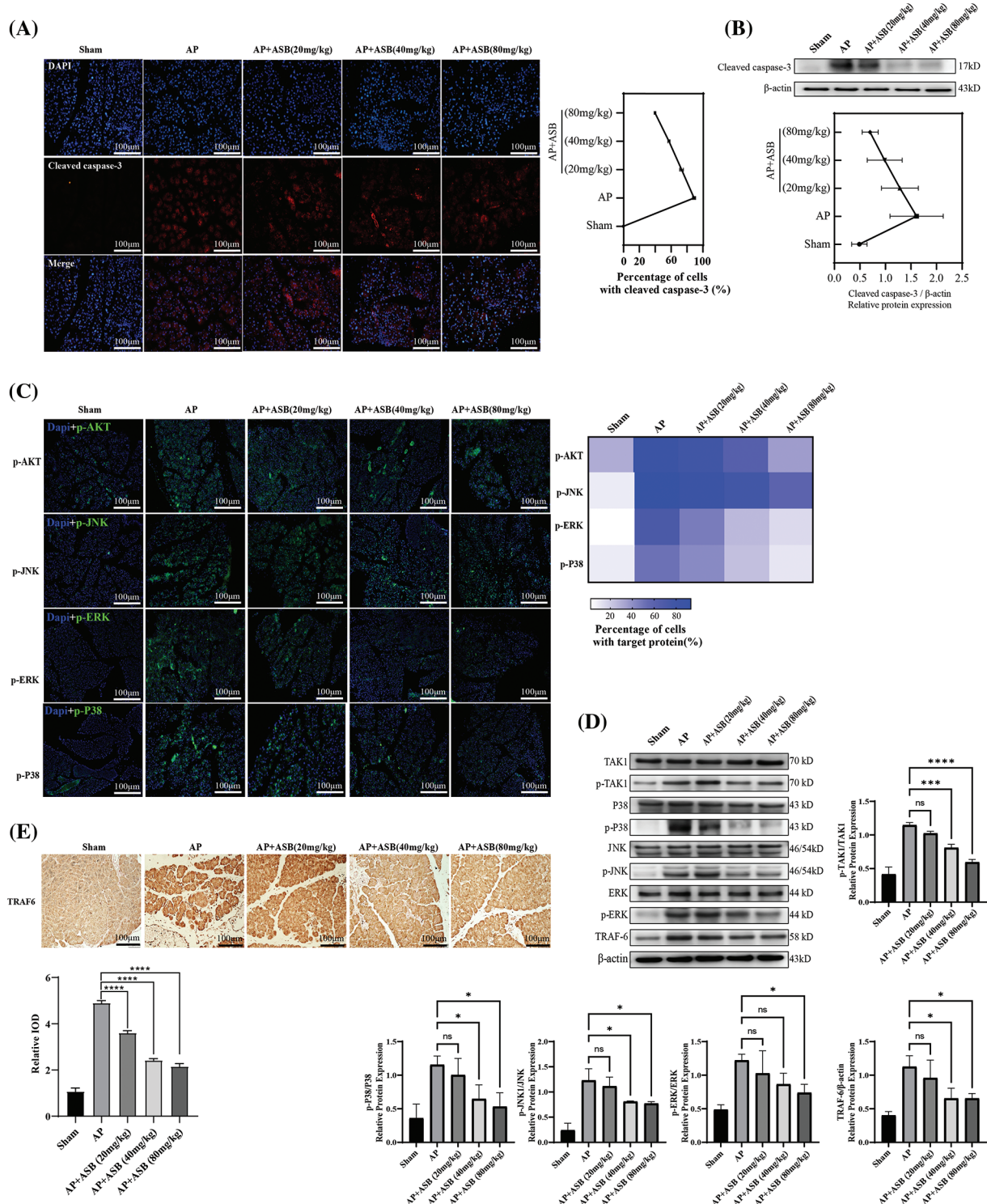


**FIGURE 3.** ASB mitigates apoptosis in acute pancreatitis mice model by modulating MAPK signaling pathways. (A) Immunofluorescence detection of cleaved caspase-3 expression in pancreatic tissue. (B) Western blot analysis depicting caspase-3 protein expression in pancreatic tissue, accompanied by digital results. (C) Immunofluorescence detection of pTAK, pJNK, pERK, and pP38 in pancreatic tissue under varying treatments. (D) Detection and quantification of the expression and phosphorylation levels of key factors in the MAPK-related pathways, with digital results. (E) Immunohistochemical detection of TRAF6 in pancreatic tissue under different treatments. “ns” denotes no significant difference, \* $p < 0.05$ , \*\*\* $p < 0.001$ , \*\*\*\* $p < 0.0001$ . Scale bar = 100 μm (n = 6 mice per group).

*ASB mitigates apoptosis in AP mouse model by modulating MAPK signaling pathways*

Immunofluorescence staining in this study highlighted a significant escalation in apoptosis among pancreatic cells within the acute pancreatitis (AP) model, induced by a combination of caerulein and LPS. Notably, treatment with

ASB effectively reduced the incidence of apoptosis in pancreatic histiocytes, as depicted in Fig. 3A. To provide further insights, the extent of apoptosis in pancreatic tissues was quantified using Western blot analysis. This method confirmed the effectiveness of ASB in decreasing pancreatic tissue apoptosis, as shown in Fig. 3B. Moreover, the study

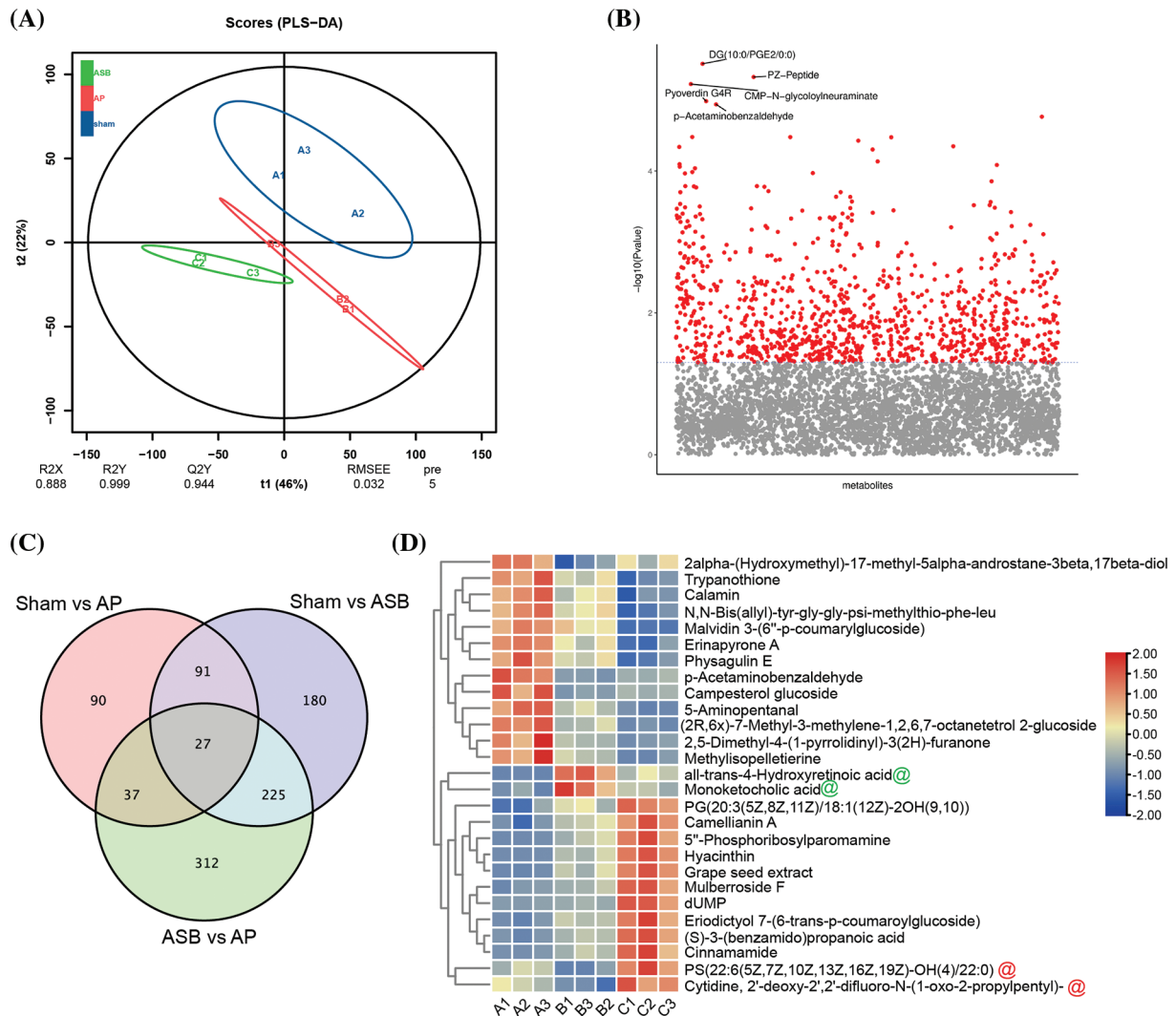


**FIGURE 4.** Overall analysis of differential metabolites. PLS-DA Plot. (A) Distinct clustering of groups represented by different colors: Blue: Sham group (Sham); Red: Acute Pancreatitis model group (AP); Green: ASB-treated group (ASB, 40 mg/kg). (B) Variance Analysis of Metabolomic Profiles. Metabolites represented on the x-axis and  $-\log_{10} p$ -values on the y-axis. Gray marks metabolites above a significance threshold, while red indicates higher relevance below the threshold. Key metabolites (DG, PZ-Peptide, Pyoverdin, CMP-N-glycolylneuraminic acid, p-Acaminobenzaldehyde) identified with the lowest  $p$ -values. (C) Venn Diagram Analysis. Red Circle: DEMs between Sham and AP model groups. Purple Circle: DEMs between Sham and ASB-treated group. Green Circle: DEMs between AP model and ASB-treated group. (D) Heat map of hub differentially expressed metabolites (Hub DEMs).

involved assessing key signaling factors associated with apoptosis through Western blotting. The results indicated that the AP model, induced by caerulein and LPS, enhanced the phosphorylation levels of TAK, p38, JNK, and ERK proteins, and increased the expression of TRAF6, as illustrated in Fig. 3C. However, both pre- and post-induction treatment with ASB successfully reduced the phosphorylation of these proteins. The findings from immunofluorescence staining of pancreatic tissue aligned with the Western blot results, as shown in Fig. 3D. Compared to the AP model, ASB markedly lowered the expression of the TRAF6 protein. This reduction was further corroborated by the immunohistochemical analysis of pancreatic tissue, demonstrating that ASB could decrease TRAF6 expression in the pancreas (Fig. 3E). These results collectively suggest a substantial therapeutic potential of ASB in mitigating apoptosis and modulating key signaling pathways in the context of AP.

#### Overall analysis of differential metabolites by ASB treatment

In this study, to elucidate the regulatory effects of ASB on the MAPK signaling pathway and apoptosis, we conducted a metabolomic analysis of pancreatic tissues from the sham, AP, and ASB-treated (40 mg/kg) groups. The Partial Least Squares Discriminant Analysis (PLS-DA) plot revealed distinct separations among these three groups, with each clustering into their own unique groups (Fig. 4A). This differentiation indicates significant metabolic variations induced by AP and modulated by ASB treatment. Variance analysis of the metabolomic profiles highlighted differences in metabolite levels between the groups. On the plot, the x-axis represents the metabolites, while the y-axis shows the  $-\log_{10} p$ -value. Metabolites above a certain significance threshold were marked in gray, and those below the threshold, indicating higher relevance, were colored in red. Key metabolites, such as DG, PZ-Peptide, Pyoverdin, CMP-N-glycolylneuraminic acid, and p-Acaminobenzaldehyde,

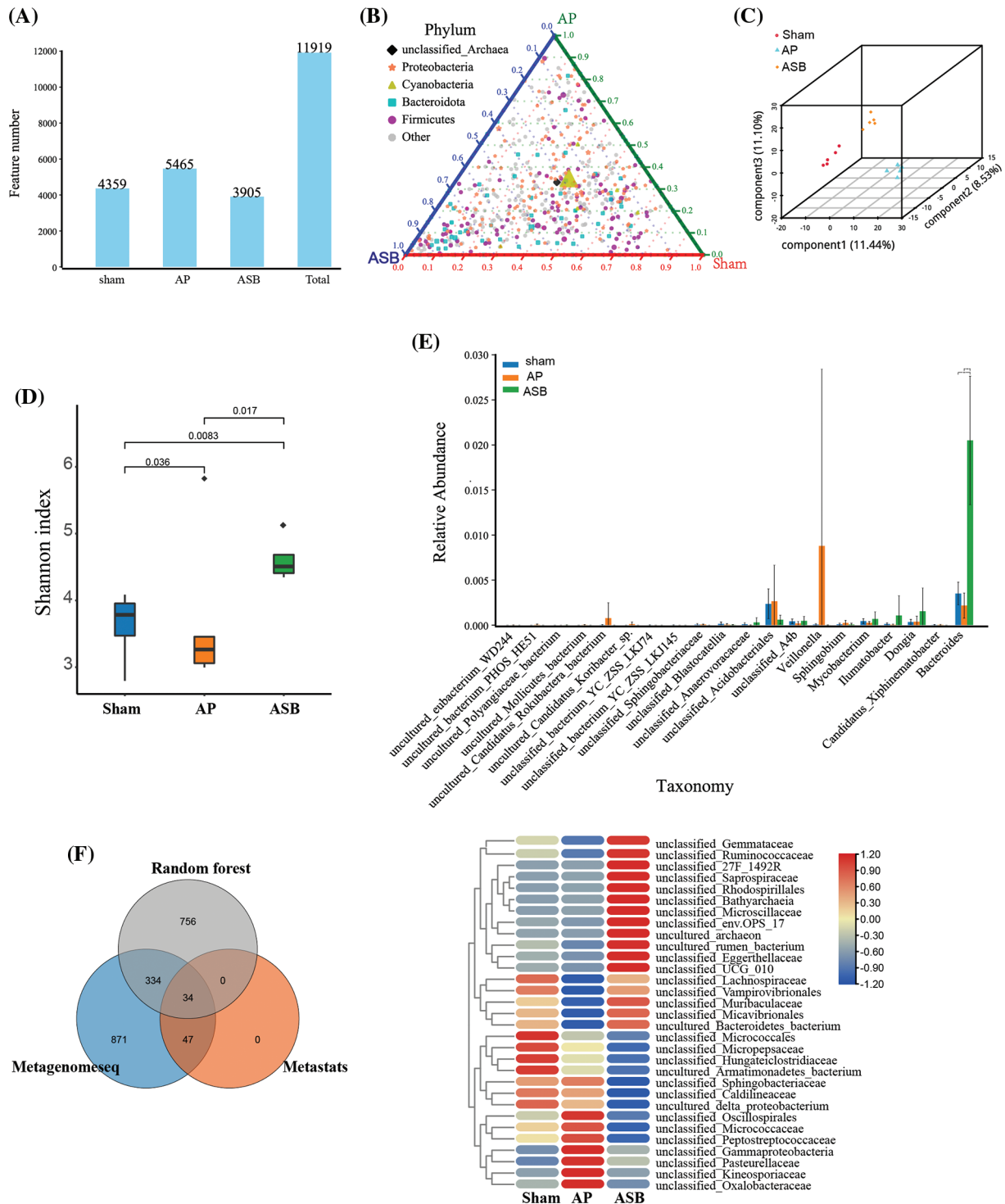


**FIGURE 5.** Microbial diversity analysis in model after ASB treatment. (A) OTU abundance analysis. The distribution of OTUs in the corresponding sample. (B) Ternary phase diagram analysis. Each of the three angles represents a sample and the three edges of the triangle measure the relative abundance of species for the corresponding-colored samples. The legend in the plot displays colored shapes representing the top five genus levels with the highest abundances. (C and D). Alpha diversity analysis. Graphs depicting distinct clustering among the three study groups, illustrating the diversity within each group. (E) ANOVA analysis (genus). (F) Venn analysis of differential species and Heat map of hub species. The Venn diagram illustrates the outcomes of metagenomic data analyzed through three distinct analytical models. Specifically: Gray circles represent results obtained using the Random Forest algorithm. Blue circles denote results achieved through the Metagenomeseq method. Orange circles indicate results generated with the Metastats approach.

were identified with the lowest  $p$ -values (Fig. 4B). A Venn diagram analysis further identified 27 differentially expressed metabolites (DEMs) common across all three groups (Fig. 4C). Subsequent heatmap analysis of these

DEMs provided deeper insights. Notably, metabolites like all-trans-4-Hydroxyretinoic acid and Monoketochoic acid were found to be significantly elevated in the AP group but showed a marked decrease following ASB treatment.

Conversely, PS (22:6(5Z,7Z,10Z,13Z,16Z,19Z)-OH(4)/22:0) and Cytidine, 2'-deoxy-2',2'-difluoro-N-(1-oxo-2-propylpentyl), which were reduced in the AP group, exhibited a significant increase after ASB intervention (Fig. 4D). These findings underscore the potential of ASB in modulating specific metabolic pathways affected in AP, offering insights into its therapeutic mechanism.

#### *Microbial diversity analysis in the model after ASB treatment*

The burgeoning recognition of the gut microbiota's role in the onset and treatment of AP guided our investigation into how ASB affects this intricate microbial ecosystem. Microbial sequencing of our study samples revealed that the total number of Operational Taxonomic Units (OTUs) was significantly greater in the AP group compared to the sham group. Interestingly, these OTUs were notably lower in the ASB-treated group, suggesting a modulatory effect of ASB on gut microbiota diversity in AP (Fig. 5A). In our ternary phase diagram analysis, Cyanobacteria were centrally positioned, skewing towards the sham and AP groups, while Firmicutes and Bacteroidota showed a deviation towards the AP and ASB groups, indicating shifts in microbial populations (Fig. 5B). Alpha diversity analysis further highlighted distinct clustering among the three groups, showcasing the diversity within each (Figs. 5C, 5D). An ANOVA analysis at the genus level revealed significant microbial differences between the AP and ASB-treated groups. Notably, the genus *Veillonella* was more prevalent in the AP group, potentially linking it to AP pathology. Conversely, the ASB-treated group exhibited an increase in *Bacteroides*, suggesting a correlation with ASB's therapeutic effects in AP (Fig. 5E). Moreover, a Venn diagram identified 34 common differentially expressed species across the groups. Heatmap analysis of these species showed that families like Oxalobacteraceae, Kineosporiaceae, Pasteurellaceae, and Gammaproteobacteria were significantly increased in the AP group. Conversely, families such as Lachnospiraceae, Vampirovibrionales, Muribaculaceae, Micavibrionales, and Bacteroidetes\_bacterium were more abundant in the sham and ASB-treated groups but decreased in the AP group (Fig. 5F). These findings suggest that AP induces significant alterations in the gut microbiota, and ASB treatment effectively modulates these changes, shedding light on the dynamic interaction between gut microbiota and AP, and the potential role of ASB in restoring microbial balance during AP treatment.

#### *Correlation analysis linking metabolites and microbial diversity*

To delve deeper into the mechanisms by which ASB influences metabolic and microbial responses in AP, our study integrated a module-to-module analysis. This involved constructing heatmaps to examine the relationships between metabolites and microbial groups (Fig. 6A). Following this, we employed total correlation and Canonical Correspondence Analysis (CCA) to identify key hub metabolites and microbial species (Figs. 6B, 6C). The analysis revealed several microbial groups as potential targets influenced by ASB treatment. These included unclassified members of the Saprospiraceae, Micavibrionales, Ruminococcaceae, and

Kineosporiaceae families. In terms of metabolites, we noted significant changes in response to ASB treatment. Particularly, LysoPE (0:0/20:0), PC (DiMe (13,5)/PGJ2), Heptanoic acid, Cytidine (2'-deoxy-2',2'-difluoro-N-(1-oxo-2-propylpentyl)), and Lithocholic acid were found to be elevated in the ASB-treated group. Moreover, the metabolite CAY10616 was observed to increase in the AP group but showed a significant decrease in the ASB-treated group (Fig. 6D). These findings suggest a complex interplay between ASB treatment and the host's metabolic and microbial environment in the context of AP. The study highlights the potential of ASB in modulating both gut microbiota and metabolic profiles, thereby offering insights into its therapeutic mechanisms in AP.

## **Discussion**

Acute pancreatitis (AP) is a prevalent clinical condition characterized by a high incidence rate and the potential for both acute symptoms and long-term complications [2]. Currently, there is a notable gap in the availability of effective treatments for AP. In this context, traditional Chinese medicine, known for its anti-inflammatory properties, presents a promising avenue for the development of new treatments for AP. Anemarsaponin B (ASB) has shown certain anti-inflammatory properties in cellular level experiments [15]. This study was designed to investigate the therapeutic potential of ASB in AP. We induced an AP model in mice using a combination of caerulein and LPS and then administered ASB. Our objective was to elucidate the molecular mechanisms underlying the effects of ASB in the treatment of AP, thereby contributing to the development of new therapeutic strategies for this condition.

After administering a combination of caerulein and LPS to induce AP in mice, significant changes were observed in key AP-related indicators. Specifically, levels of pancreatic enzymes, esterase and amylase, were markedly elevated compared to those in the sham group ( $p < 0.01$ ). This increase in enzyme levels is a characteristic marker of AP. Furthermore, Hematoxylin and Eosin (H&E) staining of the pancreatic tissues revealed extensive infiltration of inflammatory cells, and serum levels of inflammatory cytokines such as IL-1 $\beta$ , IL-6, and TNF- $\alpha$  were significantly heightened ( $p < 0.01$ ). In contrast, the levels of anti-inflammatory redox factors, namely Superoxide Dismutase (SOD) and Glutathione Peroxidase (GSH), were found to be reduced ( $p < 0.01$ ). These findings corroborate the induction of an AP model in mice, aligning with the research results of Heath, Li, and others [23–25]. Interestingly, H&E staining of the intestinal tissues indicated that AP could lead to structural remodeling of the small intestinal villi. Given the rapid turnover rate of these villi [26], the deeper mechanisms underlying this observation warrant further investigation. It is important to note that results can vary depending on the methods used to induce AP.

Treating mice with ASB both before and after the induction of AP with caerulein and LPS has shown notable anti-inflammatory effects. This treatment regimen led to a reduction in serum levels of pancreatic enzymes esterase and amylase, as well as a decrease in pro-inflammatory



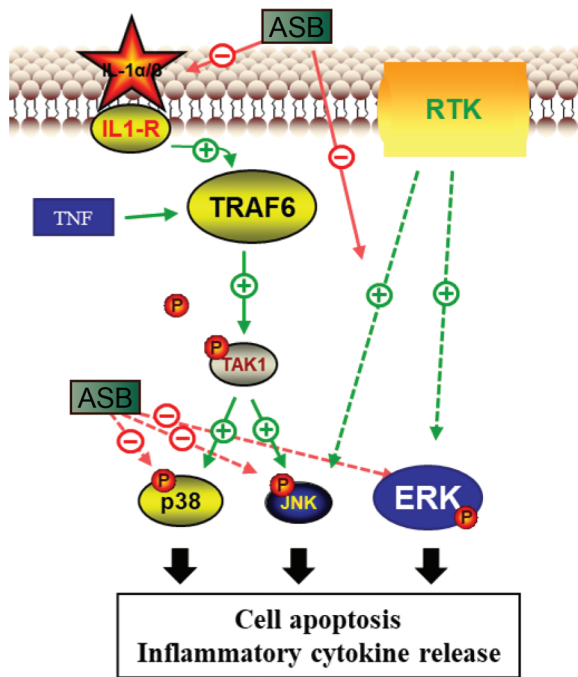


**FIGURE 7.** Pharmacological mechanism of ASB in the treatment of acute pancreatitis. ASB reduces IL-1 $\alpha$  secretion of MAPK, inhibits the phosphorylation levels of key proteins TAK, JNK, ERK, and P38 in MAPK-related pathways, and alleviates cell apoptosis and immune inflammatory effects.

pathway [15]. Western Blot analysis also demonstrated that ASB reduces the phosphorylation of JNK and p38.

Furthermore, IL-1 activates the TNF signaling pathway via IL-1R, inducing TRAF6 expression, which in turn increases TAK protein phosphorylation, activating p38 and affecting cell apoptosis [18,27,28]. This study highlights the significant role of ASB in the IL1-induced MAPK pathway, as evidenced by the reduced serum levels of IL-1 $\beta$  and the protein TRAF6 in comparison to the AP model group. Additionally, the decreased levels of cleaved Caspase-3 following ASB treatment indicate its potential to alleviate cell apoptosis.

Our sequencing analysis highlighted that the bacterial families or orders Saprospiraceae, Micavibrionales, Ruminococcaceae, and Kineosporiaceae were up-regulated in the ASB treatment group compared to both the AP and normal groups. These bacteria may impact host cell apoptosis and MAPK pathways through various mechanisms, potentially involving the production of toxins or metabolic by-products [29]. However, the specific roles of these bacterial groups in relation to apoptosis or MAPK pathways require further detailed investigation, as their functions can be highly nuanced and context dependent.

Additionally, our study identified several metabolites associated with these bacterial groups. LysoPEs (Lysophosphatidylethanolamines) are lipid molecules that may play a role in apoptosis and MAPK pathways [30], acting as lipid signaling molecules that can affect cellular processes including cell death and signaling. PC(DiMe(13,5)/PGJ2), a phosphatidylcholine derivative, could be implicated in lipid signaling or metabolism. The component PGJ2 (Prostaglandin J2) is known for its involvement in

inflammatory responses and may influence apoptosis and MAPK pathways [31]. Heptanoic Acid, a medium-chain fatty acid, may induce oxidative stress or modulate signaling pathways [32]. Its specific role in MAPK pathways is less clear but might relate to energy metabolism and signaling. The modified nucleoside, Cytidine, 2'-deoxy-2',2'-difluoro-N-(1-oxo-2-propylpentyl), could impact apoptosis through its integration into DNA or RNA, thereby affecting genetic stability or expression [33]. Its influence on MAPK pathways is likely indirect, potentially through gene expression effects. Lithocholic Acid, a secondary bile acid (SBA), has been shown to induce apoptosis in certain cell types and can be involved in signaling pathways, including the MAPK pathway [34,35]. Interestingly, a significant correlation between bile acid levels and the abundance of Ruminococcaceae has been observed in previous research [36]. Ruminococcaceae is known to include SBA-producing bacteria, crucial for converting primary bile acids to SBAs. Our findings suggest that ASB treatment increases secondary bile acids, potentially by regulating Ruminococcaceae abundance. This regulation could attenuate the MAPK signaling pathway, leading to reduced apoptosis. This study underscores the complex interplay between ASB treatment, gut microbiota, and associated metabolic profiles in the context of AP. It reveals potential mechanisms through which ASB may exert therapeutic effects, including modulation of bacterial populations and metabolic pathways linked to apoptosis and MAPK signaling. LysoPEs, PC(DiMe(13,5)/PGJ2), Heptanoic Acid, the modified nucleoside Cytidine, and Lithocholic Acid were among the metabolites found to be influenced by ASB treatment. These findings elucidate the molecular mechanisms behind the AP model induction by caerulein and LPS and suggest the potential mechanisms of ASB's efficacy in alleviating AP symptoms. They further affirm ASB's therapeutic promise for AP and provide a new direction for clinical research into traditional Chinese medicine treatments for AP.

## Conclusion

ASB has demonstrated considerable anti-inflammatory potential, positioning it as a viable candidate for clinical treatments and combination therapies for AP. However, it is imperative to conduct further toxicological and pharmacodynamic studies to ensure its safety and efficacy. AP is known to trigger a cascade of inflammatory responses, characterized by the production of cytokines such as IL-1, IL-6, and TNF- $\alpha$ . These cytokines can induce cell apoptosis through various pathways, including the TNF signaling pathway and the MAPK signaling pathway. This study highlights ASB's ability to effectively inhibit the MAPK pathway, thereby decelerating the process of cell apoptosis. Within the MAPK pathway, JNK, p38, and ERK serve as key downstream signaling molecules. JNK and p38 are primarily activated by IL-1, while ERK is activated through the RTK-MAPK-ERK pathway. Additionally, analysis of microbiota and metabolic pathways suggests that ASB treatment can lead to changes in microbial communities and metabolites associated with apoptosis and the MAPK

pathway in AP. These findings underscore ASB's role in mitigating the inflammatory symptoms of AP and elucidate the molecular mechanisms behind its therapeutic action (Fig. 7), providing a valuable foundation for future drug development. Further research using diverse models of AP induction is necessary to fully understand ASB's mechanism of action and its broader applicability. This will enable the development of more effective treatment strategies tailored to different contexts.

**Acknowledgement:** We are grateful to the participants who generously dedicated their time and effort to contribute to our study. Our appreciation also extends to the laboratory staff for their valuable technical assistance, and to the funding agency for providing the necessary resources for conducting this research. Finally, we acknowledge the anonymous reviewers whose insightful comments and suggestions significantly enhanced the quality of this manuscript.

**Funding Statement:** This work was sponsored by Natural Science Foundation of Chongqing, China (cstc2021jcyj-msxmX0724; cstc2020jcyj-msxmX0434) and Chongqing Key Specialty Fund of Clinical Pharmacy.

**Author Contributions:** The authors confirm contribution to the paper as follows: conceptualization, data curation, formal analysis, investigation, methodology, validation, and manuscript writing: Yi Hu and Zhongyang Ren; investigation, resourcing, and visualization: Zhengzhong Zhao; data curation, investigation, validation, and visualization: Yongjia Huang and Wanting Huang; project administration, resourcing, supervision, and manuscript writing: Jie Liu and Ling Ding. All authors reviewed the results and approved the final version of the manuscript.

**Availability of Data and Materials:** The datasets generated and analyzed during this study are available from the corresponding author upon reasonable request. These data are not publicly accessible due to privacy and ethical considerations.

**Ethics Approval:** Full compliance with the animal welfare and ethical requirements of Chongqing Liangjiang New District, as authorized by the IV/S-SYDW-045 approval number, is mandatory for all experimental animals involved in this project.

**Conflicts of Interest:** The authors declare that they have no conflicts of interest to report regarding the present study.

## References

- Guo Y, Hu W, Wang X, Li C, Cui T, Liu R, et al. PSD-95 protects the pancreas against pathological damage through p38 MAPK signaling pathway in acute pancreatitis. *Exp Biol Med*. 2021;246(13):1473–82.
- Mederos MA, Reber HA, Girgis MD. Acute pancreatitis: a review. *JAMA*. 2021;325(4):382–90.
- Gukovskaya AS, Pandol SJ, Gukovsky I. New insights into the pathways initiating and driving pancreatitis. *Curr Opin Gastroenterol*. 2016;32(5):429–35.
- Gerasimenko JV, Gryshchenko O, Ferdek PE, Stapleton E, Hebert TO, Bychkova S, et al. Ca<sup>2+</sup> release-activated Ca<sup>2+</sup> channel blockade as a potential tool in antipancreatitis therapy. *Proc Natl Acad Sci USA*. 2013;110(32):13186–91.
- Wen L, Voronina S, Javed MA, Awais M, Szatmary P, Latawiec D, et al. Inhibitors of ORAI1 prevent cytosolic calcium-associated injury of human pancreatic acinar cells and acute pancreatitis in 3 mouse models. *Gastroenterol*. 2015;149(2):481–92.
- Biczo G, Vegh ET, Shalbueva N, Mareninova OA, Elperin J, Lotshaw E, et al. Mitochondrial dysfunction, through impaired autophagy, leads to endoplasmic reticulum stress, deregulated lipid metabolism, and pancreatitis in animal models. *Gastroenterol*. 2018;154(3):689–703.
- Javed MA, Wen L, Awais M, Latawiec D, Huang W, Chvanov M, et al. TRO40303 ameliorates alcohol-induced pancreatitis through reduction of fatty acid ethyl ester-induced mitochondrial injury and necrotic cell death. *Pancreas*. 2018;47(1):18–24.
- Zeng Y, Wang X, Zhang W, Wu K, Ma J. Hypertriglyceridemia aggravates ER stress and pathogenesis of acute pancreatitis. *Hepatogastroenterol*. 2012;59(119):2318–26.
- Griffith JW, Sokol CL, Luster AD. Chemokines and chemokine receptors: positioning cells for host defense and immunity. *Annu Rev Immunol*. 2014;32(1):659–702.
- Watanabe T, Kudo M, Strober W. Immunopathogenesis of pancreatitis. *Mucosal Immunol*. 2017;10(2):283–98.
- Bentham J. Worldwide trends in body-mass index, underweight, overweight, and obesity from 1975 to 2016: a pooled analysis of 2416 population-based measurement studies in 128.9 million children, adolescents, and adults. *Lancet*. 2017;390(10113):2627–42.
- Li XY, He C, Zhu Y, Lu NH. Role of gut microbiota on intestinal barrier function in acute pancreatitis. *World J Gastroenterol*. 2020;26(18):2187–93.
- Yang BY, Zhang J, Liu Y, Kuang HX. Steroidal saponins from the rhizomes of *Anemarrhena asphodeloides*. *Molecules*. 2016;21(8):1075.
- Qin L, Han T, Zhang Q, Cao D, Nian H, Rahman K, et al. Antiosteoporotic chemical constituents from Er-Xian decoction, a traditional Chinese herbal formula. *J Ethnopharmacol*. 2008;118(2):271–9.
- Kim JY, Shin JS, Ryu JH, Kim SY, Cho YW, Choi JH, et al. Anti-inflammatory effect of anemarsaponin B isolated from the rhizomes of *Anemarrhena asphodeloides* in LPS-induced RAW 264.7 macrophages is mediated by negative regulation of the nuclear factor- $\kappa$ B and p38 pathways. *Food Chem Toxicol*. 2009;47(7):1610–7.
- Dong JX, Han GY. A new active steroidal saponin from *Anemarrhena asphodeloides*. *Planta Med*. 1991;57(5):460–2.
- Liu X, Xiang D, Jin W, Zhao G, Li H, Xie B, et al. Timosaponin B-II alleviates osteoarthritis-related inflammation and extracellular matrix degradation through inhibition of mitogen-activated protein kinases and nuclear factor- $\kappa$ B pathways in vitro. *Bioengineered*. 2022;13(2):3450–61.
- Shi K, Zhu J, Chen D, Ren C, Guo M, Wang J, et al. Lipidomics analysis of timosaponin BII in INS-1 cells induced by glycolipid toxicity and its relationship with inflammation. *Chem Biodivers*. 2020;17(4):e1900684.
- Lu WQ, Qiu Y, Li TJ, Tao X, Sun LN, Chen WS. Timosaponin B-II inhibits pro-inflammatory cytokine induction by

- lipopolysaccharide in BV2 cells. *Arch Pharm Res.* 2009;32(9):1301–8.
20. Guo C, Li L, Yang X, Meng Z, Li F, Zhang C, et al. Protective effects of timosaponin B-II on high glucose-induced apoptosis in human umbilical vein endothelial cells. *Environ Toxicol Pharmacol.* 2014;37(1):37–44.
  21. Wu X, Yao J, Hu Q, Kang H, Miao Y, Zhu L, et al. Emodin ameliorates acute pancreatitis-associated lung injury through inhibiting the alveolar macrophages pyroptosis. *Front Pharmacol.* 2022;13:873053.
  22. Han X, Li B, Bao J, Wu Z, Chen C, Ni J, et al. Endoplasmic reticulum stress promoted acinar cell necroptosis in acute pancreatitis through cathepsinB-mediated AP-1 activation. *Front Immunol.* 2022;13:968639.
  23. Heath H, Britton G, Kudo H, Renney G, Ward M, Hutchins R, et al. Stat2 loss disrupts damage signalling and is protective in acute pancreatitis. *J Pathol.* 2020;252(1):41–52.
  24. Zhang PY, Yu B, Men WJ, Bai RY, Chen MY, Wang ZX, et al. Acetyl- $\alpha$ -boswellic acid and Acetyl- $\beta$ -boswellic acid protects against caerulein-induced pancreatitis via down-regulating MAPKs in mice. *Int Immunopharmacol.* 2020;86(12):106682.
  25. Li B, Wu J, Bao J, Han X, Shen S, Ye X, et al. Activation of  $\alpha$ 7nACh receptor protects against acute pancreatitis through enhancing TFEB-regulated autophagy. *Biochim Biophys Acta Mol Basis Dis.* 2020;1866(12):165971.
  26. Clevers HC, Bevins CL. Paneth cells: maestros of the small intestinal crypts. *Annu Rev Physiol.* 2013;75(1):289–311.
  27. McDermott EP, O'Neill LA. Ras participates in the activation of p38 MAPK by interleukin-1 by associating with IRAK, IRAK2, TRAF6, and TAK-1. *J Biol Chem.* 2002;277(10):7808–15.
  28. Zhu W, Li W, Jiang J, Wang D, Mao X, Zhang J, et al. Chronic salmon calcitonin exerts an antidepressant effect via modulating the p38 MAPK signaling pathway. *Front Mol Neurosci.* 2023;16:1071327.
  29. Wang X, Yu N, Wang Z, Qiu T, Jiang L, Zhu X, et al. Akebia trifoliata pericarp extract ameliorates inflammation through NF- $\kappa$ B/MAPK signaling pathways and modifies gut microbiota. *Food Funct.* 2020;11(5):4682–96.
  30. Zhang W, Liu C, Wang M, Yang Z, Yang J, Ren Y, et al. Phosphatidylserine-specific phospholipase A1 alleviates lipopolysaccharide-induced macrophage inflammation by inhibiting MAPKs activation. *Biol Pharm Bull.* 2022;45(8):1061–8.
  31. Choi J, Suh JY, Kim DH, Na HK, Surh YJ. 15-Deoxy- $\Delta^{12,14}$ -prostaglandin J<sub>2</sub> induces epithelial-to-mesenchymal transition in human breast cancer cells and promotes fibroblast activation. *J Cancer Prev.* 2020;25(3):152–63.
  32. Sun H, Zhang L, Wang Z, Gu D, Zhu M, Cai Y, et al. Single-cell transcriptome analysis indicates fatty acid metabolism-mediated metastasis and immunosuppression in male breast cancer. *Nat Commun.* 2023;14(1):5590.
  33. Lima GF, Lopes RO, Mendes A, Brazao SC, Aufran LJ, Motta N, et al. Inosine, an endogenous purine nucleoside, avoids early stages of atherosclerosis development associated to eNOS activation and p38 MAPK/NF- $\kappa$ B inhibition in rats. *Eur J Pharmacol.* 2020;882:173289.
  34. Liang H, Estes MK, Zhang H, Du G, Zhou Y. Bile acids target proteolipid nano-assemblies of EGFR and phosphatidic acid in the plasma membrane for stimulation of MAPK signaling. *PLoS One.* 2018;13(8):e198983.
  35. Liu J, Wei Y, Jia W, Can C, Wang R, Yang X, et al. Chenodeoxycholic acid suppresses AML progression through promoting lipid peroxidation via ROS/p38 MAPK/DGAT1 pathway and inhibiting M2 macrophage polarization. *Redox Biol.* 2022;56(4):102452.
  36. Zhang T, Sun P, Geng Q, Fan H, Gong Y, Hu Y, et al. Disrupted spermatogenesis in a metabolic syndrome model: the role of vitamin A metabolism in the gut-testis axis. *Gut.* 2022;71(1):78–87.